tvst

Article

Normative Data of Axial Length, Retinal Thickness Measurements, Visual Evoked Potentials, and Full-Field Electroretinography in Female, Wild-Type Minipigs

Kwang-Eon Choi[1], Vu Thi Que Anh[2], Jong-Hyun Oh[3], Cheolmin Yun[1], and Seong-Woo Kim[1]

[1] Department of Ophthalmology, Korea University College of Medicine, Seoul, Korea
[2] Department of Ophthalmology, Hanoi Medical University, Hanoi, Vietnam
[3] Department of Ophthalmology, Dongguk University Ilsan Hospital, Goyang, Korea

Correspondence: Seong-Woo Kim, Department of Ophthalmology, Korea University Guro Hospital 148, Gurodong-ro, Guro-gu, Seoul, South Korea. e-mail: ksw64723@korea.ac.kr

Received: February 25, 2021
Accepted: August 22, 2021
Published: October 4, 2021

Keywords: minipig; retina; visual streak; spectral-domain optical coherence tomography (SD-OCT); electrophysiology

Citation: Choi KE, Anh VTQ, Oh JH, Yun C, Kim SW. Normative data of axial length, retinal thickness measurements, visual evoked potentials, and full-field electroretinography in female, wild-type minipigs. Transl Vis Sci Technol. 2021;10(12):3, https://doi.org/10.1167/tvst.10.12.3

Purpose: The purpose of this study was to present normative data of optical coherence tomography (OCT), electrophysiological, and ocular biometry parameters and their correlation in minipigs.

Methods: Eighty-eight eyes of 44 minipigs underwent full-field electroretinogram (ERG) recording and ocular biometry. However, 10 eyes of 6 minipigs were excluded because of poor OCT image quality. The thickness of the retinal sublayers was measured on a vertical line at 5 locations with a 1 mm interval from the disc margin to the dorsal periphery and at 10 locations on the visual streak. Visual evoked potentials (VEPs) were measured in 15 eyes of 8 minipigs.

Results: All minipigs were female with a mean age and axial length of 13.83 $\pm$ 10.56 months and 20.33 $\pm$ 0.88 mm, respectively. The implicit time of the a-wave and b-wave in scotopic 3.0 ERGs was longer than that in photopic 3.0 ERG. The implicit time of the n2-wave and p2-wave in VEP was 25.67 $\pm$ 7.41 ms and 52.96 $\pm$ 10.38 ms, respectively. The total retinal layer (TRL) and nerve fiber layer (NFL) became thinner near the periphery. The inner retinal sublayers near the visual streak were thicker than those at other locations. Central TRL and NFL thickness on visual streak was 223.06 $\pm$ 23.19 µm and 74.03 $\pm$ 13.93 µm, respectively. The temporal TRL and NFL on the visual streak were thicker than those on the nasal side.

Conclusions: The normative electrophysiological and OCT parameters used in our study can be used as reference data in further pig studies.

Translational Relevance: This study presents normative data of minipigs, which are adequate animal models for preclinical studies.

Introduction

Large animal models are needed for the development of new drugs and ocular devices for human eye diseases.[1–3] Normative data are essential to observe the significant changes after experiments or intervention.[1,4–6] Pig and human eyes share many anatomic similarities that make the former useful in ophthalmic research.[7,8] The size of a pig eyeball (21.64–23.9 mm) is comparable to that of a human eyeball (23–24 mm), which is larger than those of a mouse (approximately 3 mm), rat (6–7 mm), rabbit (approximately 16 mm), and dog (18–19 mm).[9–16] Pigs also have a visual streak where photoreceptors and ganglion cell layers are concentrated and showed a high rod and cone cell density ranging from 83,000 to 200,000 cells/mm^2.[2,17,18] These features make pigs a good candidate for evaluating various therapeutic strategies, such as stem cell therapy, gene therapy, and implantation of retinal prosthesis, for photoreceptor degeneration.

To investigate morphological and functional retinal changes, optical coherence tomography (OCT) with

a fundus camera and electrophysiological tests, such as electroretinogram (ERG) and visual evoked potential (VEP) examinations, are popular among laboratory researchers. In particular, the correlation between OCT and functional findings is useful for optic nerve disease or retinal degeneration.[19–21] OCT is enables a noninvasive examination of the retina and choroid with high resolution.[1,2,22,23] OCT data have proven useful in various animal experiments.[24,25] Several pig studies about the correlations between OCT and histological results have been conducted.[1,2] Furthermore, the clinical significance and reliability of OCT images have been established.[1,2,26] Several animal studies have shown that the total thickness of the retina decreases as the distance from the optic disc increases.[24,27–29] However, there is a paucity of OCT studies that have focused on the thickness of each sublayer in pigs,[1,26] particularly in the visual streak. ERG and VEP tests are representative tests for the detection of visual function. Such electrophysiological tests can be useful in quantifying the possible effects in experimental ophthalmologic studies,[30–32] and there have been some studies of ERGs in pigs.[33–35]

Therefore, in the present study, we report the thickness of each retinal layer in various locations according to the distance from the optic disc and along the visual streak in wild-type minipigs. Normative data on ocular biometry and electrophysiology were also evaluated.

Materials and Methods

ERG and OCT examinations were performed on minipigs (MICROPIG T-type, Sus scrofa domestica; APURES Co., Ltd, Pyeongtaek-si, Korea). All minipigs that underwent ERG examination were enrolled. To evaluate the peripheral location adequately, OCT images of good quality were used for the analysis. For VEP examination, one eye of one normal minipig and 14 eyes of 7 normal minipigs before euthanasia were enrolled. All evaluations for each minipig were performed while they were under general anesthesia, and the method of general anesthesia was as follows. The minipigs were anesthetized by intravenous injection of alfaxalone (1 mg/kg of Alfaxan; Vetoquinol, West Sussex, UK) into the marginal auricular vein following premedication, which comprised a subcutaneous injection of atropine (0.05 mg/kg) and an intramuscular injection of xylazine (1 mg/kg of Rompun; Bayer Corp., Shawnee Mission, KS, USA) and azaperone (4 mg/kg of Stresnil; Mallinckrodt Veterinary Inc., Indianapolis, IN, USA), sequentially. After the induction of general anesthesia, maintenance was performed using 1.5% to 2.5% isoflurane at 2 L/min with 50% to 70% oxygen supply. The eyes were dilated with three eyedrops of a tropherine solution (phenylephrine hydrochloride 5 mg/mL + tropicamide 5 mg/mL) after general anesthesia. After 3 consecutive loadings of eye drops, dilating eye drops were administered at 30-minute intervals.

All procedures adhered to the Association for Research in Vision and Ophthalmology's Statement for the Use of Animals in Ophthalmic and Vision Research. Approval for this study was obtained from the Institutional Animal Care and Use Committee of the Korea University College of Medicine.

Ocular Biometry

Axial length (AL), anterior chamber depth, lens thickness, and vitreous chamber depth were measured in both eyes using commercial biometry (SW-1000 A-scan ultrasonography; Suoer, Shanghai, China). The data were obtained using an automatic averaging program with 10 measurements. The lid speculum was inserted, and an emulsion fluid was applied to the cornea. The applanation probe was then placed on the corneal center of each pig eye with minimal pressure by a retina specialist (author K.E.C.).

Electroretinography

The ERG protocol was based on the international standard for electroretinography from the International Society for Clinical Electrophysiology of Vision (ISCEV).[36,37] The stimulus strengths for scotopic ERG examination were 0.01, 3.0, and 10 cd·seconds·m^{-2}, and those for the photopic ERG examination were 0.01, 3.0, 10, and 3.0 cd·seconds·m^{-2}. The inner stimulus times for scotopic 0.01, 3.0, and 10.0 ERG examinations were 0.49, 0.1, and 0.05 Hz, respectively. The inner stimulus times for the photopic 3.0 ERG and 30 Hz flicker ERG examination were 2.0 Hz and 30 Hz, respectively. The background-light strength of photopic ERG examination was 30 cdm^{-2}, and recording bandpass was 0.3 to 300 Hz. Sixteen responses with a 2-second interstimulus interval were obtained for each recording and averaged. The pupils were dilated up to 5 mm in diameter under general anesthesia, and then dark adaptation was performed for 30 minutes. The dilatation of the pupil was maintained by topical eye drops with 30-minute intervals until the end of the experiment. Light-emitting diode (LED) light stimulation was modulated, and ERG signal recording was performed using a

commercial system (RETIcom; Ronald Consult, Germany). A contact lens electrode with a built-in LED light source (Kooijman/Damhof ERG lens; Medical Workshop BV, The Netherlands) was used for light stimulation, which provided consistent illumination.[38] During the experiments, the pupils remained dilated, and the contact lens electrode was kept in contact with the eye using hypromellose. The obtained responses were transferred to a computer system for data storage and printing of the recordings. Reference and ground electrodes were subdermal platinum needle electrodes. Reference electrodes were placed in the skin near the lateral canthus of the eyes, and a ground electrode was placed on the forehead between the two eyes.

Flash Visual Evoked Potentials

The skull of a pig is quite thick, and there is a sinus between the skull and brain.[39,40] Therefore, it is nearly impossible to obtain a VEP by placing a skin electrode upon or under the skin, as in humans. A hole was drilled in the cranium, and an electrode was grounded to the epidural surface for VEP evaluation. First, a superior-inferior view and lateral view of a head radiograph were obtained to check the brain location. Second, we made a sufficiently long vertical incision in the skin and muscle above the visual cortex on the opposite side (the periphery at a 2 cm distance from the center) of the eye to expose the skull adequately. Third, a round craniotomy was performed at the planned location using a commercial neurosurgery drill (Anspach BlackMax; Johnson & Johnson, New Brunswick, NJ, US) with a 14 mm Codman perforator. Drilling was performed with water sprinkling until the bone was completely penetrated, and then the drill was turned away. Then, the thin bone seen under the sinus was tapped and broken using a surgical hammer.[41] The epidural surface was visible when the broken bone was removed with forceps. A recording electrode patch was placed on the epidural surface, and cotton gauze was used to fill the space to keep the electrode in contact with the epidural surface. Finally, the skin was sutured. For the reference electrode, a craniotomy was performed on the frontal lobe site in the same manner, and the reference electrode was placed on the epidural surface of the frontal lobe (Fig. 1). A needle electrode for the ground signal was inserted into the skin of the anterior leg. The flash VEP protocols were based on the ISCEV standard,[42] with a stimulus luminance of 3.0 cd·seconds·m^{-2} and a recording bandpass was 1 to 500 Hz. VEP stimulation

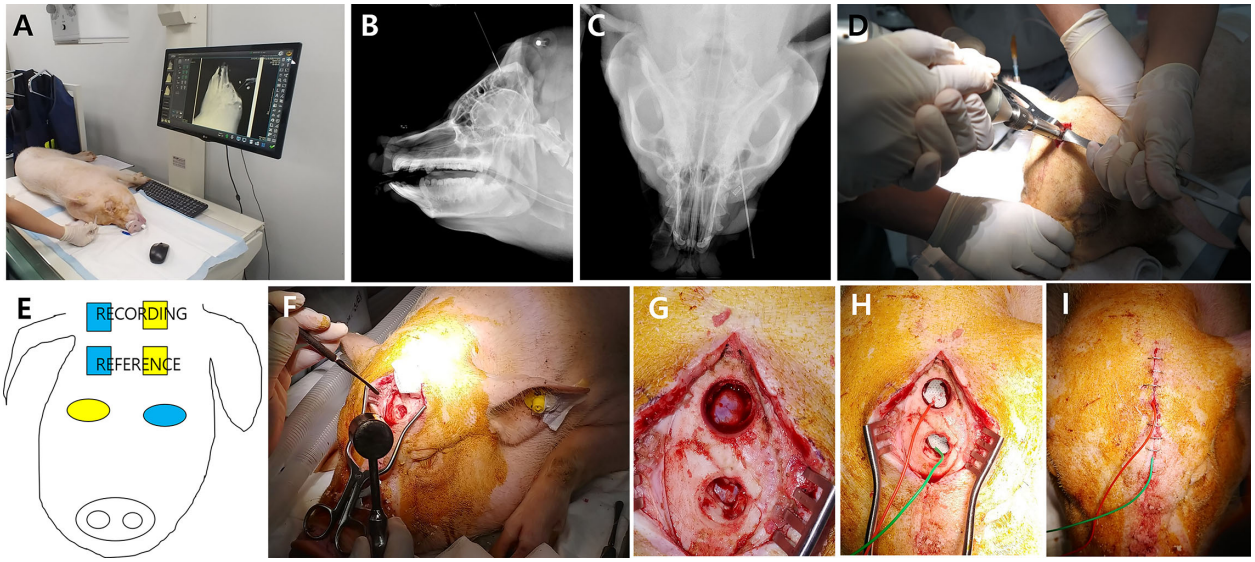

Figure 1. Preparation for the Evaluation of Visual Evoked Potentials (VEP). (**A**) Confirmation of the brain location is done by taking a lateral view (**B**) and a superior-inferior view (**C**) radiograph of the head. **C** A radiographic image of a minipig head with a needle penetrating deep into the skin at the occipital cortex is shown. (**D**) A sufficiently long incision is made in the skin and muscle to expose the skull base. (**E**) Schematic planning to punch the skull with a neurosurgery drill above the visual cortex for a recording electrode and frontal lobe as a reference electrode is shown. The recording electrode is targeted contralateral to the eye side of VEP stimulation. (**F**) A round-shaped craniotomy is performed using a neurosurgery drill at the planned location. (**G**) The epidural surface is visible after removing the thin bone shown below using a surgical hammer and chisel following the first craniotomy. (**H**) The patch recording electrode is placed on the epidural surface and the space above it is filled with cotton gauze to keep the electrode in contact with the epidural surface. (**I**) Resuturing of the skin is performed.

was performed with a RETIcom machine using a contact lens with a built-in light source. After induction of deep anesthesia using ketamine (50 mg/kg) and xylazine (10 mg/kg), euthanasia was performed by collecting whole blood.

Image Acquisition and Analysis

Using a Spectralis OCT machine (Heidelberg Engineering GmbH, Heidelberg, Germany), infrared images and OCT images in the 55 degree range were obtained. Vertical and horizontal line scans and raster scans (33 B-scans for a 16.5 × 16.5 mm area in a 55 degree image) were performed in high-resolution mode (1536 A-scans per B scan, lateral resolution of 10 µm/pixel for a 55 degrees image). Up to 100 single images were averaged using an automatic real-time mode to obtain a high-quality average image (Fig. 2C). The measurements were manually performed by a retinal specialist (author K.E.C.) and a general ophthalmologist (author V.T.Q.A.). Intercorrelation scores were measured. Moreover, the data from the retinal specialist (K.E.C.) were used for analysis. The measurement was performed at several points of a vertical line from the optic disc margin between the two dorsal large blood vessels from the optic disc (Fig. 2A). The thickness of each sublayer was measured on the vertical line at distances of 1, 2, 3, 4, and 5 mm from the optic disc margin (see Fig. 2A). The thickness of the total retinal layer (TRL), total choroidal layer (CL), nerve fiber layer (NFL), ganglion cell complex (GCC), ganglion cell layer (GCL), inner plexiform layer (IPL), GCL/IPL, inner nuclear layer (INL), outer plexiform layer (OPL), outer nuclear layer (ONL), inner retinal layer (IRL), and outer retinal layer (ORL) was measured manually. TRL was defined as the layer from the inner border of the internal limiting membrane (ILM) to the outer border of the retinal pigment epithelium (RPE) cell layer. CL was defined as the layer from the outer border of the RPE to the outer border of the large choroidal blood vessel. The thickness of each sublayer with low or high signal intensity in OCT images was measured directly. IRL was defined as the layer from the inner border of the ILM to the external limiting membrane (ELM). ORL was defined as the layer from the ELM to the outer border of the RPE. Additionally, the GCC was defined as the layer from the inner border of the NFL to the inner border of the INL. Finally, the GCL/IPL thickness was measured by subtracting the thickness of NFL from that of the GCC.

The visual streak is a dorsal horizontal band where the thickness of the ganglion cell density is the most abundant and vascular arcade is absent, similar to the fovea in humans.[9,17,43–45] In this study, the thickness of the horizontal line crossing at the 2 mm point of the vertical line was assumed to be the visual streak thickness (Fig. 2B). Five additional measurements were performed along this horizontal line at distances of 1 mm toward the nasal and temporal sides. Each sublayer was measured at each location. Additionally, we attempted to compare each sublayer's thickness on the nasal and temporal sides by taking an average of five measurements for each of the five locations on each side (see Fig. 2).

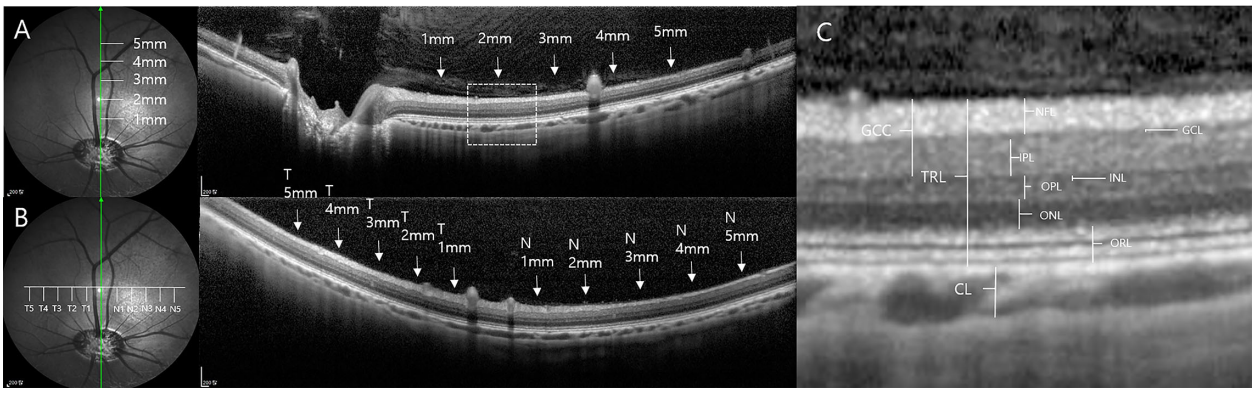

Figure 2. Representative 55 degree Optical Coherence Tomography (OCT) Images Used for Measuring Each Sublayer at Various Locations. (**A**) The vertical line is located within the vertical vein and the artery from the disc. Each point is at an interval of 1 mm. Various retinal layer thickness is measured at a total of five points on the vertical line. (**B**) The horizontal line is perpendicular to the vertical line at a point 2 mm from the disc margin. From the median line, the points are spaced at 1 mm intervals. Various retinal layer thickness are measured at five nasal points (N) and five temporal points (T) along the horizontal line. (**C**) Enlarged image from the dotted box **A**. The thickness of the total retinal layer (TRL), total choroidal layer (CL), ganglion cell complex (GCC), nerve fiber layer (NFL), ganglion cell layer (GCL), inner plexiform layer (IPL), GCL/IPL, inner nuclear layer (INL), outer plexiform layer (OPL), outer nuclear layer (ONL), inner retinal layer (IRL), and outer retinal layer (ORL) are measured manually at each location.

Correlation Among Various Parameters

Correlation was evaluated among OCT indicators, ocular biometry indices, and ERG findings To assess the relationship between ocular biometry indices and ERG findings, we used the mean sublayer thickness for analysis and each implicit time from ERGs.

Statistical Analysis

Repeated analysis of variances (ANOVA), paired *t*-tests, Pearson χ^2 tests, Pearson's correlation analyses, and multiple regression analyses were performed using SPSS version 21.0. A *P* value less than 0.05 was considered statistically significant.

Results

In total, 44 female pigs underwent ocular biometry and electrophysiological tests. The average age of the pigs was 13.83 ± 10.56 months (9–15 months), and their mean body weight was 29.66 ± 3.26 kg. The mean AL and anterior chamber depth was 20.33 ± 0.88 mm and 3.19 ± 0.42 mm, respectively (Table 1). The mean AL of the right and left eyes was 20.36 ± 1.14 mm and 20.29 ± 0.72 mm, respectively. The mean anterior chamber depth of the right and left eyes was 3.22 ± 0.45 mm and 3.16 ± 0.39 mm, respectively.

Electrophysiologic Tests

All ERGs of minipigs showed consistently similar morphology to each other (Fig. 3 and Supplementary Fig. S1). None of the ERG parameters showed any significant difference between the right and left eyes. The mean implicit time of the b-wave in scotopic 0.01 ERG was 68.09 ± 14.64 ms. The mean implicit time of the a-wave and b-wave in scotopic 3.0 ERG was 16.12 ± 3.20 ms and 41.06 ± 6.28 ms, respectively. The mean b/a ratio was 2.09 ± 0.56. The mean implicit time of the a-wave and b-wave in photopic 3.0 ERG was 13.84 ± 6.93 ms and 33.73 ± 5.78 ms, respectively. The mean implicit time and amplitudes of all waves are summarized in Table 1.

The mean age and body weight of 8 minipigs that underwent flash VEP tests were 11.26 ± 1.89 months and 27.94 ± 2.76 kg, respectively. None of the parameters showed significant differences between the right

Table 1. Electroretinography Findings ($n = 88$ Eyes)

	Both	Right Eye	Left Eye	*P* Value Between the Right Eye and Left Eye
Age (months)	13.83 ± 8.56			
Weight (kg)	64.08 ± 41.21			
AL (mm)	20.33 ± 0.88	20.36 ± 1.14	20.29 ± 0.72	0.686[a]
ACD (mm)	3.19 ± 0.42	3.22 ± 0.45	3.16 ± 0.39	0.328[a]
Lens (mm)	7.29 ± 0.69	7.33 ± 0.67	7.26 ± 0.72	0.643[b]
VCD (mm)	9.83 ± 1.23	9.79 ± 1.12	9.83 ± 1.23	0.744[b]
Mean implicit time of the b-wave in scotopic 0.01 ERGs (ms)	68.09 ± 14.64	66.67 ± 29.64	69.54 ± 15.11	0.610[b]
Mean amplitude of the b-wave in scotopic 0.01 ERGs (μV)	64.08 ± 41.21	64.36 ± 41.50	63.78 ± 41.38	0.440[b]
Mean implicit time of the a-wave in scotopic 3.0 ERGs (ms)	16.12 ± 3.20	15.77 ± 2.29	16.48 ± 3.92	0.443[b]
Mean implicit time of the b-wave in scotopic 3.0 ERGs (ms)	41.06 ± 6.28	41.02 ± 5.78	41.11 ± 6.83	0.454[b]
Mean amplitude of the a-wave in scotopic 3.0 ERGs (μV)	65.76 ± 24.68	68.13 ± 23.68	63.34 ± 25.71	0.988[b]
Mean amplitude of the b-wave in scotopic 3.0 ERGs (μV)	134.89 ± 52.21	137.34 ± 48.29	131.78 ± 56.38	0.625[b]
b/a ratio in scotopic 3.0 ERGs	2.09 ± 0.56	2.10 ± 0.55	2.08 ± 0.57	0.948[b]
Mean implicit time of the a-wave in scotopic 10.0 ERGs (ms)	15.73 ± 2.66	15.52 ± 2.38	15.95 ± 2.92	0.888[b]
Mean implicit time of the b-wave in scotopic 10.0 ERGs (ms)	40.39 ± 6.39	40.18 ± 5.69	40.61 ± 7.09	0.177[b]
Mean amplitude of the a-wave in scotopic 10.0 ERGs (μV)	56.84 ± 21.32	58.35 ± 20.26	55.30 ± 22.48	0.790[b]
Mean amplitude of the b-wave in scotopic 10.0 ERGs (μV)	109.87 ± 42.16	112.03 ± 37.59	107.65 ± 46.73	0.394[b]
Mean amplitude of oscillatory potential (μV)	19.51 ± 14.03	19.58 ± 13.25	19.45 ± 14.95	0.440[b]
Mean implicit time of the a-wave in photopic 3.0 ERGs (ms)	13.84 ± 6.93	12.65 ± 2.78	15.06 ± 9.35	0.203[b]
Mean implicit time of the b-wave in photopic 3.0 ERGs (ms)	33.73 ± 5.78	33.13 ± 4.94	34.34 ± 6.52	0.391[b]
Mean amplitude of the a-wave in photopic 3.0 ERGs (μV)	23.53 ± 12.11	23.78 ± 12.18	23.27 ± 12.18	0.760[b]
Mean amplitude of the b-wave in photopic 3.0 ERGs (μV)	131.44 ± 55.64	138.38 ± 54.67	124.35 ± 56.37	0.934[b]
Mean interval between n1 and p1 waves of photopic 3.0 flicker ERGs (ms)	21.37 ± 4.05	22.02 ± 3.55	20.70 ± 4.45	0.065[b]
Mean amplitude of photopic 3.0 flicker ERGs (μV)	114.75 ± 62.64	121.84 ± 65.01	107.51 ± 60.02	0.835[b]

AL, axial length; ACD, anterior chamber depth; VCD, vitreous chamber depth; ERG, electroretinogram.
[a]Paired *t* test.
[b]Wilcoxon signed-rank test.

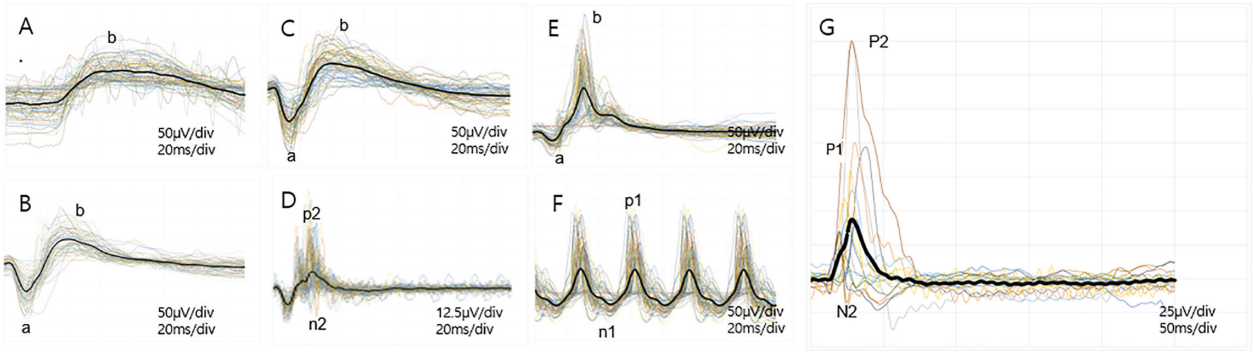

Figure 3. Overall Trace Maps of Full-field Electroretinograms (ERG) and VEP in Minipigs. Overall trace maps of full-field electroretinogram (ERG). (**A**) A scotopic 0.01 ERG is shown. The mean implicit time of the b-wave in the scotopic 0.01 ERG is 68.09 ± 14.64 ms, and the amplitude is 64.08 ± 41.21 μV. (**B**) A scotopic 3.0 ERG is show. The mean implicit time of the a-wave and b-wave is 16.12 ± 3.20 ms and 41.06 ± 6.28 ms, respectively. The amplitudes of the a-wave and b-wave are 65.76 ± 24.68 μV and 134.89 ± 52.21 μV, respectively. (**C**) A scotopic 10.0 ERG is shown. The mean implicit time of the a-wave and b-wave is 15.73 ± 2.66 ms and 40.39 ± 6.39 ms, respectively. The mean amplitudes of the a-wave and b-wave are 56.84 ± 21.32 μV and 109.87 ± 42.16 μV, respectively. (**D**) The oscillatory potential is shown. The mean amplitude of oscillatory potential is 19.51 ± 14.03 μV. (**E**) A photopic 3.0 ERG is shown. The mean implicit time of the a-wave and b-wave is 13.84 ± 6.93 ms and 33.73 ± 5.78 ms, respectively. The mean amplitudes of the a-wave and b-wave are 23.53 ± 12.11 μV and 131.44 ± 55.64 μV, respectively. (**F**) A photopic flicker ERG is shown. The mean amplitude is 114.75 ± 62.64 μV. (**G**) Overall trace map of flash VEP is illustrated. The mean implicit time of the p1 wave, n2 wave, p2 wave, and n3 wave are 27.86 ± 8.07 ms, 1.76 ± 1.45 μV, 52.96 ± 10.38 ms, 122.08 ± 38.58 ms, and 255.23 ± 62.24 ms, respectively.

Table 2. Visual Evoked Potentials ($n = 15$)

	Flash VEP
Mean implicit time of the n1 wave (ms)	6.44 ± 5.42
Mean amplitude of the n1 wave (μV)	0.86 ± 1.13
Mean implicit time of the p1 wave (ms)	15.85 ± 5.46
Mean amplitude of the p1 wave (μV)	1.09 ± 1.31
Mean implicit time of the n2 wave (ms)	25.67 ± 7.41
Mean amplitude of the n2 wave (μV)	1.34 ± 1.62
Mean implicit time of the p2 wave (ms)	52.96 ± 10.38
Mean amplitude of the p2 wave (μV)	28.52 ± 22.22
Mean implicit time of the n3 wave (ms)	122.08 ± 38.58
Mean amplitude of the n3 wave (μV)	34.49 ± 23.56
Mean implicit time of the p3 wave (ms)	255.23 ± 62.24
Mean amplitude of the p3 wave (μV)	6.22 ± 4.81
Mean implicit time of the n4 wave (ms)	372.44 ± 83.92
Mean amplitude of the n4 wave (μV)	4.99 ± 3.72
Mean implicit time of the p4 wave (ms)	451.91 ± 48.98
Mean amplitude of the p4 wave (μV)	4.93 ± 2.54

VEP, visual evoked potential.

and left eyes. The flash VEP pattern of the minipigs was not the same as that of human VEPs. A small-amplitude n2-wave was followed by a large-amplitude p2-wave (Fig. 3G). The implicit time of the n2-wave and the p2-wave was 25.67 ± 7.41 ms and 52.96 ± 10.38 ms, respectively. The implicit time and amplitudes of all waves are summarized in Table 2.

OCT Measurements

Ten eyes of six minipigs (8 eyes of 4 minipigs and one eye each of 2 minipigs) were excluded as the OCT image signal-to-noise ratio was below 0.6 or image quality was inadequate to measure thickness in the periphery. A total of 39 female pigs were included in the OCT analysis. The average age of the enrolled pigs was 12.30 ± 8.19 months (9–15 months), and their mean body weight was 29.49 ± 3.19 kg. The mean thickness of TRL, CL, NFL, GCL, IPL, INL, OPL, ONL, IRL, and ORL on the vertical line from the disc margin was 206.82 ± 30.38 μm, 180.54 ± 71.58 μm, 66.41 ± 25.24 μm, 12.34 ± 3.45 μm, 46.03 ± 8.95 μm, 20.73 ± 6.59 μm, 20.51 ± 6.94 μm, 27.36 ± 8.20 μm, 167.69 ± 32.37 μm, and 25.51 ± 5.58 μm, respectively (Table 3). There was no significant difference in thickness of any layer between the left and right eyes (all $P >$ 0.05). The mean thickness of each sublayer is summarized in Supplementary Table S1.

There were significant differences among the 5 locations at distances of 1-mm interval on the vertical line from the disc margin in TRL, NFL, GCC, GCL/IPL, IPL, INL, OPL, and ONL (all $P < 0.001$ by ANOVA test) (Table 3). In post hoc analysis, the TRL, NFL, and GCC thickness showed a decreasing pattern with increasing distance from the optic disc. However, there was no significant difference in NFL thickness at the 4 mm and 5 mm points. The thickness of GCL/IPL,

Table 3. Optical Coherence Tomography Findings for the Vertical Axis ($n = 78$)

	1 mm	2 mm	3 mm	4 mm	5 mm	Total	*P* Value
Mean TRL thickness (μm)	237.96 ± 26.27	223.06 ± 23.19	207.31 ± 18.11	189.12 ± 17.54	176.62 ± 17.54	206.82 ± 30.38	<0.001[a]
Mean NFL thickness (μm)	103.14 ± 23.07	74.03 ± 13.93	58.38 ± 8.82	51.25 ± 10.99	45.26 ± 10.77	66.41 ± 25.24	<0.001[a]
Mean GCC thickness (μm)	152.30 ± 21.77	128.52 ± 16.09	115.78 ± 14.69	100.74 ± 12.84	90.57 ± 12.52	117.58 ± 12.52	<0.001[a]
Mean GCL/IPL thickness	49.16 ± 9.49	54.49 ± 8.25	57.39 ± 10.95	49.49 ± 6.59	45.32 ± 8.24	51.17 ± 5.09	<0.001[a]
Mean IPL thickness (μm)	44.28 ± 8.01	50.41 ± 7.86	51.67 ± 7.86	43.38 ± 7.09	40.39 ± 7.76	46.03 ± 8.95	<0.001[a]
Mean INL thickness (μm)	19.01 ± 5.71	22.49 ± 6.25	23.93 ± 6.49	19.69 ± 6.68	18.56 ± 6.24	20.73 ± 6.59	<0.001[a]
Mean OPL thickness (μm)	17.91 ± 5.01	24.22 ± 6.97	22.81 ± 7.01	19.71 ± 7.00	17.89 ± 6.15	20.51 ± 6.94	<0.001[a]
Mean ONL thickness (μm)	29.32 ± 6.69	30.69 ± 7.79	29.41 ± 6.52	29.47 ± 7.26	24.25 ± 5.96	28.63 ± 7.19	<0.001[a]
Mean IRL thickness (μm)	200.62 ± 25.34	181.71 ± 24.67	169.12 ± 22.25	148.79 ± 25.14	138.21 ± 19.40	167.69 ± 32.37	<0.001[a]

TRL, total retinal layer; CL, choroidal layer; INL, inner nuclear layer; NFL, nerve fiber layer; GCC, ganglion cell complex; IPL, inner plexiform layer; INL, inner nuclear layer; OPL, outer plexiform layer; ONL, outer nuclear layer; IRL, inner retinal layer.
[a]Wilcoxon signed-rank test.

IPL, INL, and OPL at the 2 mm and 3 mm points were significantly greater than those at the 1 mm and 4 mm points (3 mm vs. 2 mm vs. 1 mm and 4 mm vs. 5 mm for GCL/IPL; 2 mm and 3 mm vs. 1 mm, 4 mm, and 5 mm for IPL, NL, and OPL). Furthermore, IPL at the 5-mm point was significantly thinner than that at the 1-mm point. ONL appeared to be thickest at the 2 mm point; however, only ONL at the 5-mm point was significantly thinner than at the other points (Supplementary Table S2, Supplementary Fig. S2, Fig. 4).

The mean thickness of TRL, CL, NFL, GCC, GCL/IPL, GCL, IPL, INL, OPL, ONL, IRL, and ORL on the horizontal line with the center point at 2 mm distance from the disc margin was 215.79 ± 24.21 μm, 183.54 ± 36.61 μm, 55.71 ± 19.40 μm, 113.52 ± 14.06 μm, 57.81 ± 7.50 μm, 12.02 ± 5.68 μm, 49.84 ± 8.36 μm, 24.79 ± 6.11 μm, 19.51 ± 6.42 μm, 30.98 ± 8.53 μm, 169.28 ± 23.66 μm, and 36.54 ± 3.41 μm, respectively The thickness of each sublayer on the presumed visual streak is summarized in Supplementary Table S3. Temporally, the thickness of TRL, IRL, GCC, and NFL were significantly greater than their nasal values ($P < 0.001$, $P = 0.001$, $P < 0.001$, and $P = 0.005$, respectively, by paired *t*-test). There were no significant differences in the thickness of the other layers between the temporal and nasal sides. The thickness of TRL, IRL, GCC, and NFL on the horizontal line showed significant differences among the 10 locations (all $P < 0.001$ by ANOVA test). After post hoc analysis, TRL at 2 mm and 1 mm on the temporal side and 1 mm on the nasal side was thicker than that at 3 mm, 4 mm, and 5 mm on the nasal side. The thickness of IRL and NFL at 2 mm and 1 mm on the temporal side and 1 mm on the nasal side was greater than that at 5 mm on the temporal side and 3 mm, 4 mm, and 5 mm on the nasal side. The GCC thickness at 2 mm and 1 mm temporally and 1 mm and 2 mm nasally was greater than that at 5 mm and 4 mm temporally and 4 mm and 5 mm nasally (see Supplementary Table S3, Supplementary Fig. S3, Fig. 4).

Correlations Among Various Parameters

To reduce bias, one minipig aged 60 months was excluded from this analysis. AL was positively correlated with anterior chamber depth ($r = 0.314$, $P = 0.004$) and vitreous chamber depth ($r = 0.792$, $P < 0.001$). AL was negatively correlated with lens thickness ($r = -0.815$, $P < 0.001$) and positively correlated with vitreous chamber thickness ($r = 0.781$, $P < 0.001$). AL had negative correlations with the thickness of TRL ($r = -0.493$, $P < 0.001$), GCC ($r = -0.388$, $P = 0.001$), GCL/IPL ($r = -0.481$, $P < 0.001$), GCL ($P = -0.272$ and $P = 0.019$), IPL ($r = -0.451$, $P < 0.001$), INL ($r = -0.415$, $P < 0.001$), OPL ($r = -0.244$, $P = 0.036$), and ONL ($r = -0.287$, $P = 0.013$). Age was significantly correlated with OPL ($r = 0.375$, $P < 0.001$). The results of multiple regression analyses using OCT parameters that showed significant correlations with ocular biometry indices (Pearson's correlation coefficient, $r > 0.3$) were as follows. The thickness of OPL showed negative correlations ($r^2 = 0.194$) with age (B = 0.459, $P = 0.001$) and AL (B = −1.190, $P = 0.037$). The correlations between ERG parameters and other factors showed low significance values (Supplementary Table S4).

Discussion

Pig and human eyes have many similarities, including a non-tapetal fundus with a holangiotic vascular pattern and retinal layer thickness. AL of mouse, rat, and rabbit eyes is much smaller than that of human eyes, which is approximately 23 to 24 mm. The minipigs used in our study had an eyeball size of 20.33 mm, similar to that in other pig studies (approximately 21 mm).[9,46,47] The anterior chamber depth in this study was greater (3.19 mm) than in another pig study using OCT and was similar to

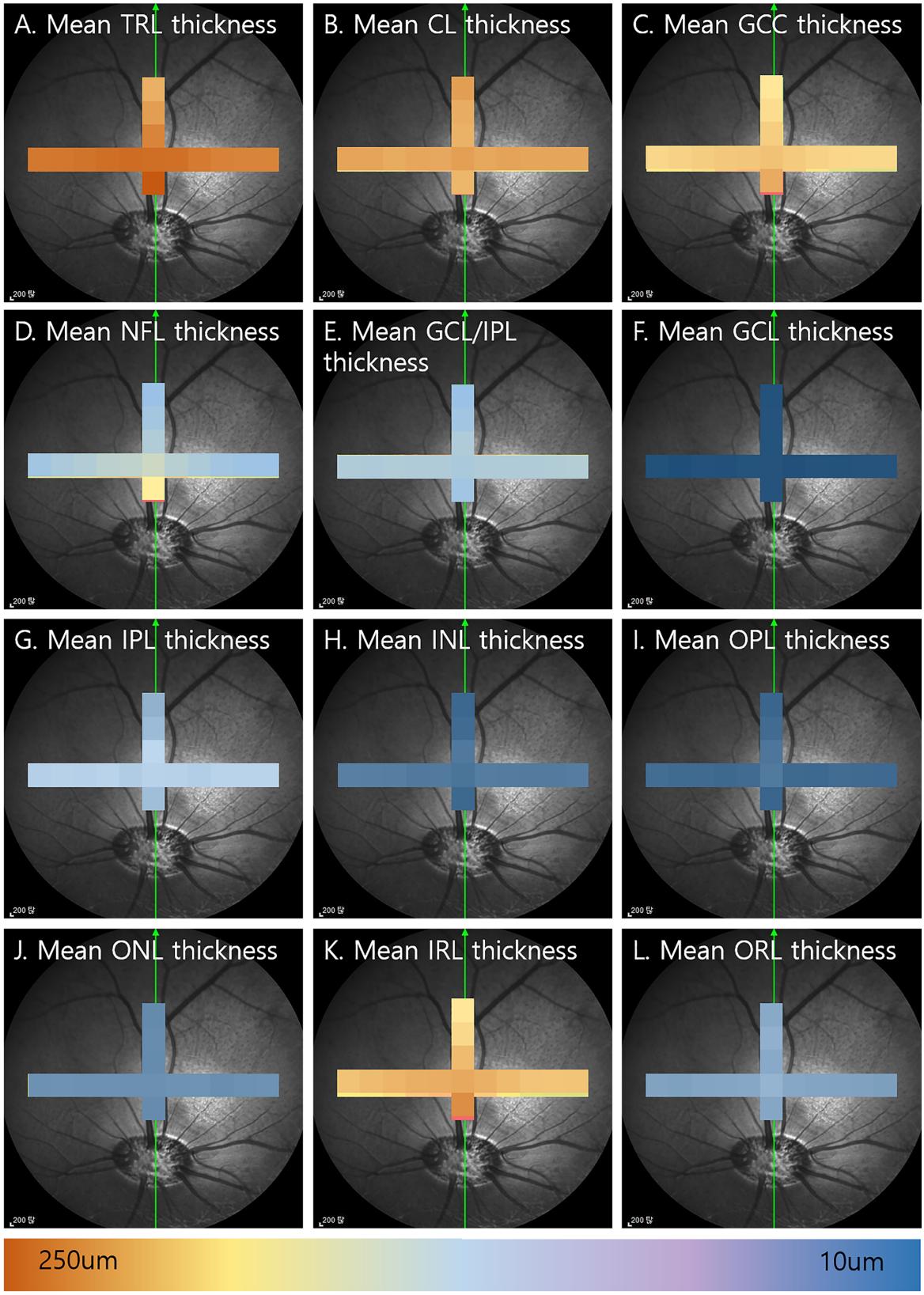

Figure 4. **Heat map showing difference thickness of each sublayer at different 15 locations.** (**A**) TRL thickness near the optic disc and vertical line is thicker than TRL thickness at other locations. (**B**) None of the CL thickness values have significant differences between them. (**C**) GCC thickness near the optic disc and vertical line is thicker than GCC thickness at other locations. (**D**) NFL thickness near the optic disc →

←
and vertical line is thicker than NFL thickness at other locations. (**E**) The GCL/IPL thickness at 2 and 3 mm from optic disc is thicker than those at 1, 4, and 5 mm. However, there is no difference of GCL/IPL thickness along the visual streak. (**F**) None of the GCL thickness values have significant differences between them. (**G**) The IPL thickness at 2 and 3 mm from optic disc is thicker than those at 1, 4, and 5 mm. However, there is no difference of IPL thickness along the visual streak. (**H**) The INL thickness at 2 and 3 mm from optic disc is thicker than those at 1, 4, and 5 mm. However, there is no difference of IPL thickness along the visual streak. (**I**) The OPL thickness at 2 and 3 mm from optic disc is thicker than those at 1, 4, and 5 mm. However, there is no difference of IPL thickness along the visual streak. (**J**) The ONL thickness at 5 mm (b) is significantly smaller than those at the other locations. (**K**) IRL thickness near the optic disc and vertical line is thicker than IRL thickness at other locations. (**L**) None of the ORL thickness values show significant differences between them.

that of humans (2.50–3.44 mm).[46,47] Pigs showed the denser photoreceptor number (20 million cones and 120 milion rods) than mice (180 thousand cones and 6.4 million rods), rabbit (8 million cones and 100 million rods), and nonhuman primates (3.1 million cones and 61 million rods).[48,49] Overall rod:cone density (7:1–8:1) in pigs is relatively lower than that in humans (20:1); however, the cone cell density (199,000 cones/mm^2) of the central area in pigs was comparable to that of humans (141,000 cones/mm^2).[50–52]

In this study, we obtained strong and stable signals with wave morphology and average amplitudes very close to those of humans and primates.[36,53,54] Minipigs showed delayed implicit time and decreased amplitudes than nonhuman primates, even though they had more large eyes and larger photoreceptor numbers than nonhuman primates.[55] It is difficult to compare directly the ERG parameters in different animals under ISCEV standard methods, because there are lots of other factors affecting ffERG, such as eyebyall sizes (size of retinal area), orbital rim thickness, location of electrodes, electodes materials, general anesthesia, and so on.[56,57] The implicit time of the a-wave (16.12 ms) and b-wave (41.06 ms) in scotopic 3.0 ERG (rod-cone response) in our study were similar to those reported by Bouskila et al. in the rod-cone response of green monkeys (14.8 ms and 36.7 ms, respectively).[58] Furthermore, our ERG results (aged 14 months and weighed 30 kg) were comparable to those of other pig studies and valuable with a relatively larger number of subjects. Previous studies of ERG using normal pig showed the a-wave implicit time (16.6 ms) in rod-cone response, b-wave implicit time (41.8–47.4 ms) in rod-cone response, a-wave implicit time (12.7–16.7 ms) in maximal rod-cone response, b-wave implicit time (36.0–45.0 ms) in maximal rod-cone response, a-wave implicit time (8.37–13.4 ms) in cone response, and b-wave implicit time (29.6–33.5 ms) in cone response.[33,34,59,60] The b-wave amplitude of 10.0 ERG in our study showed a smaller amplitude than that of 3.0 ERG.

The VEP recordings of our study showed a small-amplitude n2-wave (25.67 ms), followed by a large-amplitude p2-wave (52.96 ms) and a large-amplitude n3-wave (122.08 ms). Sachs et al. and Schwahn et al. showed similar VEP morphologies to that of our findings in epidural recordings with craniotomy in the minipig.[4,61] Using subdermal platinum needles, Barone et al. and Strain et al. reported the possibility of VEP signal detection at a relatively young age without craniotomy (n2 wave just below 0.05 seconds and p2 wave just above 0.05 seconds).[6,62] The implicit time could be affected by the visual track length and brain size.[63,64] However, recording electrodes in the above two studies without craniotomy had more distance from the eye. Therefore, the implicit time showed the tendency of delayed latency. As each pig type has different skull and brain sizes, the implicit time of each wave varies.[4,6,61,62] However, the amplitudes with craniotomy were generally larger than those without craniotomy,[63] because the distance between recording elctrodes and visual cortex were shorter with craniotomy than without craviotomy.[64] Although craniotomy is an inconvenient procedure, it is helpful to record large amplitudes to rule out noise signals from true signals. Without craniotomy, there is a possibility of failure in acquiring VEPs in adult pigs with thick neck tissue. In contrast, our study showed quantitative VEP results for minipigs with craniotomy. The VEP wave morphology in our study appeared to have a much faster implicit time than that of human fVEP (n2 approximately 90 ms, and p2 approximately 120 ms).[42,65,66] Comparing with humans, (1300 g and 15 cm) the pig can have at least 7.5 times smaller brain size (100–180 g and 7.5 cm) and the shorter distance (10–12 cm vs. 7–8 cm) between the eye and dorsal visual cortex.[67–69] In addition, the waveform and amplitudes of VEP recordings in primates were found to differ according to the depth of electrodes (deep or superficial from the brain) or recording locations in the striate laminae.[70,71] Because there were the similarities between our VEP findings and the VEP waveform of pigs using skin electrodes without craniotomies in other previous studies,[4,6,61,62] the differences in recording site (shorter than that of humans in our study) could have affected the results. It is also possible that different waveforms of each VEP originated

from species differences in the eye-to-brain signaling pathway.

Our study presented the specific thickness of each sublayer at various locations. As was shown in other studies,[24,27–29] the TRL thickness tends to decrease as it moves away from the optic disc margin. Similar tendencies were also noted for the thickness of the GCC and NFL in our study. Interestingly, the thickness of the GCL/IPL, IPL, INL, and OPL was greater near the visual streak than at other dorsal locations. Xia et al. reported the thickness of each retinal layer (TRL, NFL, GCL, IPL, INL, OPL, ONL, ellipsoid zone, and interdigitation zone/RPE were 290, 66, 18, 68, 41, 12, 39, 18, and 15 µm, respectively) at a point located 3 mm dorsally to the optic disc[26] and these values were greater than those at the same locations in our study. Using the rabbit, the outer retinal thickneess and photoreceptor outer segment thickness were thickest in the central visual streak and thinnest outside the visual streak.[72]

The visual streak with high optical cell density is located approximately 1.5 to 3 mm from the disc margin.[17,18,43,45] Deschaepdrijver et al. showed a streak-like macular area lacking major vasculature within a similar region,[73] and our presumed visual streak area (2 mm dorsally from disc margin) also showed a lack of major vasculature (see Fig. 2). The GCL thickness in our study did not show a significant difference according to the distance from the optic disc. GCL is the thinnest layer among the retinal sublayers; therefore, it may be difficult to measure precisely to detect subtle differences at each point. Instead, the GCL/IPL thickness was significantly greater at 2 and 3 mm from the optic disc than at other locations. Cone cell density shows an increase in a broad region dorsal to the optic disc that extends both nasally and temporally.[7,17,18] However, our study showed no significant differences at different points located dorsally from the optic disc in the thickness of ONL and ORL.

Furthermore, we investigated the distribution of each sublayer's thickness on the presumed visual streak. Other studies showed maximal ganglion and photoreceptor cell densities at the middle of the temporal arm of the streak.[17,18,43] This tendency was not observed in the thickness of the GCC/IPL, INL, and ONL on the visual streak. However, there were statistical differences in the average thickness of the TRL, IRL, GCC, and NFL between the nasal and temporal sides. The temporal retinal area is larger than the nasal area,[43] and it is natural that the temporal NFL is thicker than the nasal NFL, particularly near the optic disc. Beauchemin et al. showed that the temporal retina is thicker than the nasal retina in pig histology.[7] It is well known that AL increases with age in animals and humans.[74,75] AL showed a negative correlation with IRL thickness in our study. Thus, increasing AL can correlate with inner retinal thinning.[5,76,77] It has been reported that as aging progresses, inner retinal thinning and thickening of OPL with or without interdigitation zone occurs in humans.[78] Additionally, the thickness of inner retinal sublayers is reported to reflect the inner retinal functions of many ocular and systemic diseases.[79,80] Specifically, GCL/IPL and NFL thinning are associated with the delay of b-wave implicit time.[81] However, our study using normal adult minipigs showed the weak significance of correlations between ERG parameters and ocular biometry and other OCT parameters.

Our study had several limitations. First, we did not evaluate the thickness in the area ventral to the disc or at distant locations. There is a possibility that the thickness pattern could be different in the ventral and far peripheral areas. Instead, we focused on the dorsal area and the presumed visual streak. Far peripheral retinal locations are difficult to evaluate owing to their low image quality. Our minipigs were all female; therefore, further study with male minipigs will be needed to report the normative data of wild minipigs. Finally, the number of VEP examinations was low, and we only recorded contralateral signals from light stimulation even though the recording location was near the central line. This could affect the results, such as the waveform morphology or amplitudes. Further studies using a large number of VEP examinations with other examination modalities will help understand the correlations with VEP findings. Considering the discrepancy in thickness between the temporal and nasal sides of the retina, hemifield VEP or multifocal ERG will help understand the functional and anatomic correlation.

We reported normative data for minipigs using a larger number of subjects than that used in other studies and presented specific data for the thickness of each sublayer at various locations. Normative data from electrophysiological tests, such as ERG and VEP examinations in minipigs were obtained. For studies using minipigs, OCT, ERG, and VEP examinations are reliable and useful. The above findings could be used as baseline data and are considered normal values for assessing retinal degeneration in minipig models.

Acknowledgments

Supported by the Bio & Medical Technology Development Program of the NRF funded in part by the Korean government, the Ministry of Science and ICT (MSIP) (NRF-2017M3A9E2056458 and

2020R1A2C1005729), and by the Korea University Guro Hospital (O2001171).

Study design C.K.E. and K.S.W. Conduct of the study C.K.E. and A.V.T.Q. Data collection C.K.E. and O.J.H. Analysis and interpretation of the data C.K.E., Y.C.M., and K.S.W. Preparation, review, and approval of the manuscript C.K.E., A.V.T.Q., O.J.H., Y.C.M., and K.S.W.

Disclosure: **K.-E. Choi**, None; **V.T.Q. Anh**, None; **J.-H. Oh**, None; **C. Yun**, None; **S.-W. Kim**, None

References

1. Cheng J, Sohn EH, Jiao CH, et al. Correlation of Optical Coherence Tomography and Retinal Histology in Normal and Pro23His Retinal Degeneration Pig. *Transl Vis Sci Techn*. 2018;7:18.
2. Gloesmann M, Hermann B, Schubert C, Sattmann H, Ahnelt PK, Drexler W. Histologic correlation of pig retina radial stratification with ultrahigh-resolution optical coherence tomography. *Invest Ophthalmol Vis Sci*. 2003;44:1696–1703.
3. Sommer JR, Wong FL, Petters RM. Phenotypic stability of Pro347Leu rhodopsin transgenic pigs as indicated by photoreceptor cell degeneration. *Transgenic Res*. 2011;20:1391–1395.
4. Sachs HG, Gekeler F, Schwahn H, et al. Implantation of stimulation electrodes in the subretinal space to demonstrate cortical responses in Yucatan minipig in the course of visual prosthesis development. *Eur J Ophthalmol*. 2005;15:493–499.
5. Francisconi CLM, Wagner MB, Ribeiro RVP, Freitas AM. Effects of axial length on retinal nerve fiber layer and macular ganglion cell-inner plexiform layer measured by spectral-domain OCT. *Arq Bras Oftalmol*. 2020;83:269–276.
6. Barone F, Muscatello LV, Ventrella D, et al. The porcine iodoacetic acid model of retinal degeneration: Morpho-functional characterization of the visual system. *Exp Eye Res*. 2020;193:107979.
7. Beauchemin ML. The fine structure of the pig's retina. *Albrecht Von Graefes Arch Klin Exp Ophthalmol*. 1974;190:27–45.
8. Prince JH, Ruskell GL. The Use of Domestic Animals for Experimental Ophthalmology. *Am J Ophthalmol*. 1960;49:1202–1207.
9. Sanchez I, Martin R, Ussa F, Fernandez-Bueno I. The parameters of the porcine eyeball. *Graefes Arch Clin Exp Ophthalmol*. 2011;249:475–482.
10. Bartholomew LR, Pang DX, Sam DA, Cavender JC. Ultrasound biomicroscopy of globes from young adult pigs. *Am J Vet Res*. 1997;58:942–948.
11. Lozano DC, Twa MD. Development of a rat schematic eye from in vivo biometry and the correction of lateral magnification in SD-OCT imaging. *Invest Ophthalmol Vis Sci*. 2013;54:6446–6455.
12. Hughes A. A schematic eye for the rat. *Vis Res*. 1979;19:569–588.
13. Hughes A. A schematic eye for the rabbit. *Vis Res*. 1972;12:123–138.
14. Park H, Qazi Y, Tan C, et al. Assessment of axial length measurements in mouse eyes. *Optom Vis Sci*. 2012;89:296–303.
15. Liu JH, Farid H, Rapaport DH. Sympathetic nervous system plays a role in postnatal eyeball enlargement in the rabbit. *Invest Ophthalmol Vis Sci*. 2000;41:2684–2688.
16. Tuntivanich N, Petersen-Jones SM, Steibel JP, Johnson C, Forcier JQ. Postnatal development of canine axial globe length measured by B-scan ultrasonography. *Vet Ophthalmol*. 2007;10:2–5.
17. Chandler MJ, Smith PJ, Samuelson DA, MacKay EO. Photoreceptor density of the domestic pig retina. *Vet Ophthalmol*. 1999;2:179–184.
18. Hendrickson A, Hicks D. Distribution and density of medium- and short-wavelength selective cones in the domestic pig retina. *Exp Eye Res*. 2002;74:435–444.
19. Jnawali A, Lin X, Patel NB, Frishman LJ, Ostrin LA. Retinal ganglion cell ablation in guinea pigs. *Exp Eye Res*. 2021;202:108339.
20. Parisi V, Manni G, Centofanti M, Gandolfi SA, Olzi D, Bucci MG. Correlation between optical coherence tomography, pattern electroretinogram, and visual evoked potentials in open-angle glaucoma patients. *Ophthalmology*. 2001;108:905–912.
21. Sugita T, Kondo M, Piao CH, Ito Y, Terasaki H. Correlation between macular volume and focal macular electroretinogram in patients with retinitis pigmentosa. *Invest Ophthalmol Vis Sci*. 2008;49:3551–3558.
22. Sakamoto A, Hangai M, Yoshimura N. Spectral-domain optical coherence tomography with multiple B-scan averaging for enhanced imaging of retinal diseases. *Ophthalmology*. 2008;115:1071–1078.e1077.
23. Hernandez-Merino E, Kecova H, Jacobson SJ, Hamouche KN, Nzokwe RN, Grozdanic SD. Spectral domain optical coherence tomography (SD-OCT) assessment of the healthy female canine retina and optic nerve. *Veterinary Ophthalmol*. 2011;14:400–405.

24. Alkin Z, Kashani AH, Lopez-Jaime GR, Garcia HR, Humayun MS, Sadda SR. Quantitative Analysis of Retinal Structures Using Spectral Domain Optical Coherence Tomography in Normal Rabbits. *Current Eye Res*. 2013;38:299–304.
25. Lozano DC, Twa MD. Quantitative evaluation of factors influencing the repeatability of SD-OCT thickness measurements in the rat. *Invest Ophthalmol Vis Sci*. 2012;53:8378–8385.
26. Xie W, Zhao M, Tsai SH, et al. Correlation of spectral domain optical coherence tomography with histology and electron microscopy in the porcine retina. *Exp Eye Res*. 2018;177:181–190.
27. Carpenter CL, Kim AY, Kashani AH. Normative Retinal Thicknesses in Common Animal Models of Eye Disease Using Spectral Domain Optical Coherence Tomography. *Adv Exp Med Biol*. 2018;1074:157–166.
28. Yang JH, Yu SY, Kim TG, Seo KH, Kwak HW. Repeatability and Reproducibility of Spectral-Domain Optical Coherence Tomography Measurements of Retinal Thickness in Rats. *Curr Eye Res*. 2016;41:1346–1352.
29. Ferguson LR, Grover S, Dominguez JM, Balaiya S, Chalam KV. Retinal Thickness Measurement Obtained with Spectral Domain Optical Coherence Tomography Assisted Optical Biopsy Accurately Correlates with Ex Vivo Histology. *PLoS One*. 2014;9:e111203.
30. Pautler EL, Ennis SR. The effect of induced diabetes on the electroretinogram components of the pigmented rat. *Invest Ophthalmol Vis Sci*. 1980;19:702–705.
31. Yanase J, Ogawa H, Ohtsuka H. Rod and cone components in the dog electroretinogram during and after dark adaptation. *J Vet Med Sci*. 1995;57:877–881.
32. Gjorloff K, Andreasson S, Ehinger B. Standardized full-field electroretinography in rabbits. *Doc Ophthalmol*. 2004;109:163–168.
33. Luu CD, Foulds WS, Kaur C. Electrophysiological findings in a porcine model of selective retinal capillary closure. *Invest Ophthalmol Vis Sci*. 2012;53:2218–2225.
34. Jones RD, Stuart BP, Greufe NP, Landes AM. Electrophysiology and pathology evaluation of the Yucatan pig as a non-rodent animal model for regulatory and mechanistic toxicology studies. *Lab Anim*. 1999;33:356–365.
35. Janknecht P, Wesendahl T, Feltgen N, Otto T, Bach M. Steady-state electroretinograms and pattern electroretinograms in pigs. *Graefes Arch Clin Exp Ophthalmol*. 2001;239:133–137.
36. McCulloch DL, Marmor MF, Brigell MG, et al. ISCEV Standard for full-field clinical electroretinography (2015 update). *Doc Ophthalmol*. 2015;130:1–12.
37. Robson AG, Nilsson J, Li S, et al. ISCEV guide to visual electrodiagnostic procedures. *Doc Ophthalmol*. 2018;136:1–26.
38. Kooijman AC, Damhof A. ERG lens with built-in Ganzfeld light source for stimulation and adaptation. *Invest Ophthalmol Vis Sci*. 1980;19:315–318.
39. Herring SW, Decker JD, Liu ZJ, Ma T. Temporomandibular joint in miniature pigs: anatomy, cell replication, and relation to loading. *Anat Rec*. 2002;266:152–166.
40. Sauleau P, Lapouble E, Val-Laillet D, Malbert CH. The pig model in brain imaging and neurosurgery. *Animal*. 2009;3:1138–1151.
41. Guillaume O, Schmid T, Kluge K, et al. Introduction of the Anspach drill as a novel surgical driller for creating calvarial defects in animal models. *J Orthop Res*. 2019;37:1183–1191.
42. Odom JV, Bach M, Brigell M, et al. ISCEV standard for clinical visual evoked potentials: (2016 update). *Doc Ophthalmol*. 2016;133:1–9.
43. Hebel R. Distribution of retinal ganglion cells in five mammalian species (pig, sheep, ox, horse, dog). *Anat Embryol (Berl)*. 1976;150:45–51.
44. Shrader SM, Mowry RN. Histomorphometric evaluation of the Gottingen minipig eye. *Veterinary Ophthalmol*. 2019;22:872–878.
45. Garca M, Ruiz-Ederra J, Hernandez-Barbachano H, Vecino E. Topography of pig retinal ganglion cells. *J Comp Neurol*. 2005;486:361–372.
46. Rosolen SG, Rivière ML, Lavillegrand S, Gautier B, Picaud S, LeGargasson JF. Use of a combined slit-lamp SD-OCT to obtain anterior and posterior segment images in selected animal species. *Vet Ophthalmol*. 2012;15(Suppl 2):105–115.
47. Bhardwaj V, Rajeshbhai GP. Axial length, anterior chamber depth-a study in different age groups and refractive errors. *J Clin Diagn Res*. 2013;7:2211–2212.
48. Jeon C-J, Strettoi E, Masland RH. The Major Cell Populations of the Mouse Retina. *J Neurosci*. 1998;18:8936.
49. Szel A, Lukats A, Fekete T, Szepessy Z, Rohlich P. Photoreceptor distribution in the retinas of subprimate mammals. *J Opt Soc Am A Opt Image Sci Vis*. 2000;17:568–579.
50. Troilo D, Howland HC, Judge SJ. Visual Optics and Retinal Cone Topography in the Common Marmoset (Callithrix-Jacchus). *Vis Res*. 1993;33:1301–1310.

51. Wikler KC, Williams RW, Rakic P. Photoreceptor Mosaic - Number and Distribution of Rods and Cones in the Rhesus-Monkey Retina. *J Compar Neurol*. 1990;297:499–508.
52. Curcio CA, Sloan KR, Kalina RE, Hendrickson AE. Human Photoreceptor Topography. *J Compar Neurol*. 1990;292:497–523.
53. Mustafi D, Engel AH, Palczewski K. Structure of cone photoreceptors. *Prog Retin Eye Res*. 2009;28:289–302.
54. Johnson MA, Jeffrey BG, Messias AMV, Robson AG. ISCEV extended protocol for the stimulus-response series for the dark-adapted full-field ERG b-wave. *Doc Ophthalmol*. 2019;138:217–227.
55. Kostic C, Arsenijevic Y. Animal modelling for inherited central vision loss. *J Pathol*. 2016;238:300–310.
56. Kriss A. Skin ERGs: their effectiveness in paediatric visual assessment, confounding factors, and comparison with ERGs recorded using various types of corneal electrode. *Int J Psychophysiol*. 1994;16:137–146.
57. Hobby AE, Kozareva D, Yonova-Doing E, et al. Effect of varying skin surface electrode position on electroretinogram responses recorded using a handheld stimulating and recording system. *Doc Ophthalmol*. 2018;137:79–86.
58. Bouskila J, Javadi P, Palmour RM, Bouchard JF, Ptito M. Standardized full-field electroretinography in the Green Monkey (Chlorocebus sabaeus). *PLoS One*. 2014;9:e111569.
59. Augsburger AS, Haag V, Leuillet S, Legrand JJ, Forster R. Recording of the full-field electroretinogram in minipigs. *Vet Ophthalmol*. 2012;15(Suppl 2):84–93.
60. Rosolen SG, Rigaudiere F, Saint-Macary G, Lachapelle P. Recording the photopic electroretinogram from conscious adult Yucatan micropigs. *Doc Ophthalmol*. 1999;98:197–205.
61. Schwahn HN, Gekeler F, Kohler K, et al. Studies on the feasibility of a subretinal visual prosthesis: data from Yucatan micropig and rabbit. *Graefes Arch Clin Exp Ophthalmol*. 2001;239:961–967.
62. Strain GM, Tedford BL, Gill MS. Brainstem auditory evoked potentials and flash visual evoked potentials in Vietnamese miniature pot-bellied pigs. *Res Vet Sci*. 2006;80:91–95.
63. Snyder A, Issar D, Smith M. What Does Scalp EEG Coherence Tell Us About Long-range Cortical Networks? *Eur J Neurosci*. 2018;48:2466–2481.
64. Strain GM, Jackson RM, Tedford BL. Postnatal development of the visual-evoked potential in dogs. *Am J Vet Res*. 1991;52:231–235.
65. Tobimatsu S, Celesia GG. Studies of human visual pathophysiology with visual evoked potentials. *Clin Neurophysiol*. 2006;117:1414–1433.
66. Sokol S. Visually evoked potentials: theory, techniques and clinical applications. *Surv Ophthalmol*. 1976;21:18–44.
67. Weickenmeier J, Kurt M, Ozkaya E, Wintermark M, Pauly KB, Kuhl E. Magnetic resonance elastography of the brain: A comparison between pigs and humans. *J Mech Behav Biomed Mater*. 2018;77:702–710.
68. Schiefer U, Hart W. Functional Anatomy of the Human Visual Pathway. In: Schiefer U, Wilhelm H, Hart W (eds), *Clinical Neuro-Ophthalmology: A Practical Guide*. Berlin, Heidelberg: Springer Berlin Heidelberg; 2007:19–28.
69. Gizewski ER, Schanze T, Bolle I, de Greiff A, Forsting M, Laube T. Visualization of the visual cortex in minipigs using fMRI. *Res Vet Sci*. 2007;82:281–286.
70. Givre SJ, Schroeder CE, Arezzo JC. Contribution of extrastriate area V4 to the surface-recorded flash VEP in the awake macaque. *Vis Res*. 1994;34:415–428.
71. Schroeder CE, Tenke CE, Givre SJ, Arezzo JC, Vaughan HG. Striate Cortical Contribution to the Surface-Recorded Pattern-Reversal Vep in the Alert Monkey. *Vis Res*. 1991;31:1143–1157.
72. Lavaud A, Soukup P, Martin L, Hartnack S, Pot S. Spectral Domain Optical Coherence Tomography in Awake Rabbits Allows Identification of the Visual Streak, a Comparison with Histology. *Transl Vis Sci Technol*. 2020;9:13.
73. Deschaepdrijver L, Simoens P, Pollet L, Lauwers H, Delaey JJ. Morphological and Clinical-Study of the Retinal Circulation in the Miniature Pig. B: Fluorescein Angiography of the Retina. *Exp Eye Res*. 1992;54:975–985.
74. Wallman J, Adams JI, Trachtman JN. The eyes of young chickens grow toward emmetropia. *Invest Ophthalmol Vis Sci*. 1981;20:557–561.
75. Norton TT, McBrien NA. Normal development of refractive state and ocular component dimensions in the tree shrew (Tupaia belangeri). *Vis Res*. 1992;32:833–842.
76. Savini G, Barboni P, Parisi V, Carbonelli M. The influence of axial length on retinal nerve fibre layer thickness and optic-disc size measurements by spectral-domain OCT. *Br J Ophthalmol*. 2012;96:57–61.
77. Chua J, Tham YC, Tan B, et al. Age-related changes of individual macular retinal layers among Asians. *Sci Rep*. 2019;9:20352.

78. Nieves-Moreno M, Martinez-de-la-Casa JM, Morales-Fernandez L, Sanchez-Jean R, Saenz-Frances F, Garcia-Feijoo J. Impacts of age and sex on retinal layer thicknesses measured by spectral domain optical coherence tomography with Spectralis. *PLoS One*. 2018;13:e0194169.
79. Bush RA, Sieving PA. Inner retinal contributions to the primate photopic fast flicker electroretinogram. *J Opt Soc Am A Opt Image Sci Vis*. 1996;13:557–565.
80. Larsson J, Bauer B, Andreasson S. The 30-Hz flicker cone ERG for monitoring the early course of central retinal vein occlusion. *Acta Ophthalmol Scand*. 2000;78:187–190.
81. You Y, Graham EC, Shen T, et al. Progressive inner nuclear layer dysfunction in non-optic neuritis eyes in MS. *Neurol Neuroimmunol Neuroinflamm*. 2018;5:e427.